AIChE Jouranl

DOI10.1002/aic.16228

Solubility of CO_2 in three cellulose-dissolving ionic liquids.

Eduardo Pérez[*,a,b], Laura de Pablo[a,b], J. Juan Segovia[b], Alejandro Moreau[b], Francisco A. Sánchez[c], Selva Pereda[c,d], María Dolores Bermejo[a]

[a] BioEcoUva, Bioeconomy Research Institute, High Pressure Process Group, Department of Chemical Engineering and Environmental Technology, Universidad de Valladolid, Spain

[b] BioEcoUva, Bioeconomy Research Institute, Research Group TERMOCAL, Thermodynamics and Calibration, Universidad de Valladolid, Escuela de Ingenierías Industriales, Paseo del Cauce 59, E-47011 Valladolid, Spain

[c] Planta Piloto de Ingeniería Química (PLAPIQUI), Chemical Engineering Department, Universidad Nacional del Sur (UNS) - CONICET, Camino La Carrindanga Km7, 8000B Bahía Blanca, Argentina

[d] Thermodynamics Research Unit, School of Engineering, University of KwaZulu-Natal, Howard College Campus, King George V Avenue, Durban 4041, South Africa

*Corresponding author. Email: eperezve@hotmail.com

Abstract

The solubility of CO_2 in three cellulose-dissolving ionic liquids (1-ethyl-3-methylimidazolium diethylphosphate, [Emim][DEP], 1-allyl-3-methylimidazolium chloride, [Amim][Cl], and 1-butyl-3-methylimidazolium chloride, [Bmim][Cl]) at temperatures within 298 and 356 K and pressures up to 6.5 MPa was determined using a Van Ness-type apparatus (static isochoric). It was demonstrated that this device can work in isothermal and isoplethal modes, being the latter faster and more precise. Moreover, it was possible to determine CO_2 solubilities in metastable liquid [Bmim][Cl]. Experimental data were modelled using the Extended Henry's law correlation and the Group-Contribution

Received: Jun 18, 2019;Revised: Feb 26, 2020;Accepted: Mar 20, 2020

Equation of State (GC-EOS). New parameters for the binary interaction of CO_2 with ionic liquid groups were calculated.

Introduction

Ionic liquids (ILs) are attractive as green solvents due to their interesting properties such as negligible vapour pressure. Particularly interesting are those applications where ILs act as reaction media for chemical reactions.[1] Some of the reasons are that homogeneous catalysts can be immobilized in them and recovery of the products can be achieved without contamination. Moreover, certain ILs have sometimes outstanding properties as solvents being able to selectively dissolve biopolymers.[2-6] For example, some ILs based on acetate, dialkylphosplate and chloride can dissolve cellulose due to their ability to break hydrogen bonds present between molecules.[3] These ILs have been investigated to carry out cellulose processing reactions in them.[7-9]

The combination of ILs with CO_2, can bring additional advantages to the potential applications of the former. The most obvious of them is using supercritical CO_2 as extracting solvent to efficiently recover dissolved products, by-products or unreacted reactants.[10] Since solubility of IL into CO_2 is negligible, no contamination from the former is produced. Other additional advantage is that dissolved CO_2 in IL can improve its transport properties (i.e. reducing the viscosity)[11,12] or decreasing the melting point,[13,14] which enhances the liquid window. For example, Lopes et al.[7] demonstrated that addition of CO_2 improves the kinetics of the acetylation of cellulose in allylmethylimidazolium chloride ([Amim][Cl]) as well as the quality of the product.

Thus, knowledge of the phase behaviour of the system CO_2 + ILs at high pressure is of crucial importance to properly develop technologies involving these substances. CO_2 solubility in ILs has been experimentally determined by many authors using diverse techniques which can be classified in four categories: 1) Variable-volume synthetic methods[15-18] consist on a visual cell whose pressure can be controlled by changing its volume. A mixture CO_2 + IL of known overall composition is prepared and the phase transitions are visually detected in function of *P* and *T* while keeping composition constant, thus, an isopleth is measured for every experiment. These methods include variable-volume view cells and Cailletet apparatuses. 2) In the static isochoric methods[19-22] a mixture of known composition is prepared in a constant volume cell and the equilibration pressure of the biphasic system is measured at a certain temperature. Overall composition is changed by subsequent addition of CO_2 at constant temperature; therefore, isotherms (solubility vs. pressure) are determined. These methods are significantly simpler than the former because no observation system is required (unless the volume of the liquid phase is determined[22]) and the pressure does not need to be controlled, however a way to add accurately known amounts of gas is needed. 3) Gravimetrical methods:[23-25] solubility is measured in a microbalance by recording the mass gain upon CO_2 pressurization. They are simple but usually only suitable for a limited range of pressures and temperatures. 4) Analytical methods:[26] Although they are not very common, solubility can be determined by sampling and analysing the liquid phase to measure the amount of CO_2 and IL. If solubility of mixtures of gases is studied, the vapour phase must also be sampled.[21]

However, in general, these techniques are costly and time consuming. For this reason, it is always desirable to improve the versatility of the experimental methods. This means being able to operate having as much control as possible of the variables so the experimental grid is as wide as possible.

In this work solubility of CO_2 in three ILs with capacity to dissolve cellulose: 1-ethyl-3-methylimidazolium diethylphosphate ([Emim][DEP]), 1-allyl-3-methylimidazolium chloride ([Amim][Cl]) and 1-butyl-3-methylimidazolium chloride ([Bmim][Cl]) have been determined using a Van Ness-type apparatus (static isochoric). An attempt was done to improve the versatility of the experimental device by varying either temperature (isoplethal mode) or overall composition (isothermal mode). This way it is possible to measure solubility in a wider range of conditions changing another variable.

Another strategy to minimize experimental effort is the use of thermodynamic models and/or equations of state that allow prediction of unknown properties from previously obtained experimental data. As experimental methods, models must also be as versatile as possible so they can, not only be valid for other conditions, but also for estimating other properties or even other systems. In this sense, the Group Contribution Equation of State (GC-EOS)[27] has been particularly investigated for ILs because they can be classified in families according to its structure, which is similar between one another. The results were modelled using a thermodynamic model (Extended Henry's law correlation[23]) and the GC-EOS.

Experimental

Equipment

The solubility of CO_2 in ILs is determined with a built-in-home static device based in an original design of Van Ness and co-workers.[28] A scheme of the experimental equipment is displayed in Figure 1. It consists of a 200 mL stainless steel (SS 316) cell sealed with an encapsulated PFA/FKM o-ring. The top flange of the cell has three ports: one CO_2 inlet connected to a high pressure syringe pump ISCO 260D. This pump is thermostatized at a temperature around 0 ºC; the second is an outlet connected to a vacuum line and to vent and the last port is connected to a series of pressure transducers to accurately determine the pressure of the system. These transducers operate in different ranges: a Druck (PDCR-910-1422) sensor for pressures up to 2 MPa (P_L) and a Paroscientific 735 for higher pressures (T_L). Relative uncertainties are $u(P)/P = 2\times10^{-4}$ and 10^{-4} respectively. The former transducer can be isolated from the other and the cell by a high-pressure valve. The cell is immersed in a Hart Scientific 6020 thermostatic bath filled with water that controls the temperature with a good stability (0.01K). The temperature is accurately measured with two thermoresistances Pt100 connected to Automated System Laboratories model F250 indicator with an expanded uncertainty of 0.026 K (T_A and T_B). The contents of the cell are stirred by a magnetic flea moved by a magnetic stirrer located outside the cell.

Experimental procedure

A known amount of CO_2 can be introduced to the cell by means of the ISCO pump. From the difference of volume measured by the translation of the piston after and before the filling step, and the temperature of the pump, the amount of CO_2 added can be calculated using the density provided by the equation of state integrated in REFPROP® software[29]

The inner volume of the cell is calibrated at each temperature (313.15, 333.15 and 353.15 K) by adding a known amount of CO_2 to an empty cell. The accurately determined volume of the cell depended on temperature as: V / mL = 190.59 + 0.1113×T(ºC) with an uncertainty of 0.39 mL. When the pressure reaches a constant value, it is considered that the system is equilibrated, then the equilibrium pressure is recorded. The volume of the cell is determined from the density obtained by REFPROP and the mass of CO_2 added. The segment of tube between the transducer P_L and its isolating valve is also determined by pressure difference upon filling.

A typical experiment starts by filling the cell with a known amount (30 – 40 g) of IL previously dried by vacuum distillation for at least 12 hours at 60 ºC. Its mass is determined using a high precision balance (Sartorius Basic BA 310P). The cell is then hermetically sealed and evacuated from all the volatile components by applying vacuum at pressures down to 10^{-4} mbar for another 12 hours under stirring. Then, CO_2 is loaded into the cell by means of the ISCO pump and let for several hours under stirring until the thermodynamic equilibrium is reached. The pressure and temperature of the bath are recorded and a new point can be started. At this point there are two options: operating the device in isothermal or isoplethal mode.

In the isothermal mode, the temperature is kept constant and a new load of CO_2 is added. The time to wait is at least 12 hours but depending on the temperature or the amount loaded, this equilibration time could be higher. Further additions are done until a series of equilibration pressures are determined at a fixed temperature.

On the other hand, in the isoplethal mode, no further CO_2 additions are done apart from the first one; that is, the overall composition remains constant. Instead, the temperature of the bath is varied. The equilibration time was found to be shorter than for the isothermal mode (at least 8 hours). In this case, points of the solubility binodal at different *P* and *T* are recorded.

In principle, the device could be operated in both modes for a single load of IL, under two restrictions: a) only CO_2 additions are possible (the method was not tested for CO_2 subtractions). b) No or little hysteresis should be observed when operating under isoplethal mode.

Solubility of CO_2 in IL can be calculated by an iterative procedure assuming that the vapour phase is composed of pure CO_2.[10] Total mass in the liquid phase is the sum of the loaded mass of IL plus the mass of CO_2 dissolved, $w^L_{CO_2}$ (unknown, initial guessing, $w^L_{CO_2,0}$). The next iteration, $w^L_{CO_2,1}$ can be calculated as:

$$w^L_{CO_2,1} = w_{CO_2} - w^V_{CO_2} = w_{CO_2} - \rho_{CO_2} V^V = w_{CO_2} - \rho_{CO_2}(V - V^L)$$
$$= w_{CO_2} - \rho_{CO_2}\left(V - \frac{w^L}{\rho^L}\right) = w_{CO_2} - \rho_{CO_2}\left(V - \frac{\left(w^L_{CO_2,0} + w^L_{IL}\right)}{\rho^L}\right) \quad (1)$$

Where w_{CO_2} and $w^V_{CO_2}$ are the total mass of CO_2 added and in the vapour phase respectively. w^L_{IL} is the mass of IL in the liquid phase, which corresponds to the total mass of IL loaded. V^L, V^V and *V* are the volumes of the liquid phase, vapour phase and total respectively, the latter previously determined in the calibration stage. ρ_{CO_2} is the density of CO_2 (the vapour phase). ρ^L is the density of the saturated liquid. Upon iteration, the value for $w^L_{CO_2}$ is determined and the molar fraction of CO_2 in IL calculated.

Analysis of Uncertainty

A detailed analysis of the uncertainties was done for the experimental procedure applying the law of propagation of uncertainties to the algorithm used to calculate the composition of the liquid phase (equation 1). A summary for the uncertainty of each variable is presented in table 1.

Contributions to uncertainty in solubility measurements are considered to be the mass of IL and CO_2 loaded, the calibration of the cell volume and the density of the liquid and gas phases. The uncertainty of the CO_2 added in each measurement is determined from the uncertainties of the density of the CO_2 liquid (which depends of *T* and *P* of the pump) and the uncertainty of the volume added. During an isotherm, as subsequent additions are done, the uncertainties must also be sequentially added.

The overall uncertainty depends on the conditions of the measurement and the amount of CO_2 additions in each case, and it is represented in Figure 2 as $u(x_{CO2})$ vs. *P*. It increases with pressure reaching a maximum of 0.0076 MPs at 5.4 MPa. Figure 2a shows the evolution of the overall uncertainty along an isothermal measurement whereas figure 2b shows it along an isopleth. The contributions of each source are also represented. Both figures, 2a and 2b, show that the contribution of the uncertainty in the calibration is almost linearly dependant on the measurement pressure, which is expectable because, at higher densities, the mass of CO_2 in the phase gas under or overestimated is larger.

The uncertainty in the density of the liquid phase was estimated from the standard deviation from a linear regression to data from reference 19 and fixed to a value of 1%. Its

contribution to the overall uncertainty was also significant. This method thus requires a reasonably accurate estimation of the density for the saturated liquid.

Contribution of the uncertainty of the CO_2 additions upon an isothermal measurement increases quickly being almost the only contribution to the total uncertainty at low pressures. Along the isoplethal measurement (figure 2b), however, this contribution is significantly lower and constant because only one addition is done at the beginning of the experiment.

Thus, although improvements would be convenient in the calibration procedure, isoplethal mode is more precise than the isothermal one. Contributions of the uncertainty of the density of the gas phase and of the IL load are very small and practically negligible.

Results and discussion

In this work, densities for the system CO_2 + [Emim][DEP] were obtained from reference 20. For the system CO_2 + [Amim][Cl], densities were taken from reference 11. For the system CO_2 + [Bmim][Cl], densities were approximated to those for the pure IL.[30] Densities for the gas phase were calculated from REFPROP[29] with the temperature and pressure of the cell.

System CO_2 + [Emim][DEP]. Validation of the experimental procedure

Four experimental sets of data for the solubility of CO_2 in [Emim][DEP] were measured. Three isotherms at 313.15, 333.15 and 353.15 K and one isopleth at overall CO_2 concentration of z_{CO_2} = 0.674 (mol/mol). The results are gathered in Table 2.

The isopleth was measured at temperatures starting from 356.02 to 298.55 K. In order to evaluate the possibility of a hysteresis, i.e. if the data are equally reproducible upon

decreasing the temperature than upon increasing it, some points were repeated from 298.55 to 353.27 K. Results are represented in figure 3.

Notice that very low hysteresis is observed when increasing temperature for the system studied. The maximum difference was found at 353.27 K and 5.9 MPa and it was only 1.5%, concluding that isoplethal mode is suitable for determining solubilities within this experimental error. Lower hysteresis has been found for systems where the solubility is lower.

Figure 4 displays the solubility data for the three isotherms measured along with the isopleth. The lines for the results of the theoretical modelling are also represented.

Measured solubilities for the system CO_2 + [Emim][DEP] were compared to values in literature in order to assess the validity of this method. A deviation plot can be found in figure 5. The results agree reasonably well with data by Ramdin et al.[16] since in most cases the differences are lower than 10%. The agreement with data by Mejía et al[19] at 333.15 K is also good but not that much at 313.15 K, with a maximum deviation of almost 35%. The differences between these sets of data may be caused by differences in purity of IL but the fact of using a different type of method (isochoric instead of synthetic) could contribute, as it has previously observed in high-pressure phase equilibria [31]

System CO_2 + [Amim][Cl]

Solubilities for CO_2 in [Amim][Cl] were determined at 333.15 and 353.15 K. Results are gathered in Table 3 and plotted in Figure 6. Isotherm at 313.15 K was not measured because the melting point of this IL lies at higher temperature.[13] Solubility of CO_2 in [Amim][Cl] is significantly lower than in [Emim][DEP].

System CO_2 + [Bmim][Cl]

For the system CO_2 + [Bmim][Cl] an isotherm at 333.15 and two isopleths at overall composition z_{CO_2} of 0.538 and 0.674 were measured. In this case, these three curves were determined using the same IL load. At T = 353.15 K and from P = 0, half isotherm was measured by subsequent additions of CO_2 until z_{CO_2} = 0.538. Then the first isopleth was determined by decreasing T down to 305.95 K. Next, T was increased back to 353.15 K and the isotherm was completed until P = 5.072 MPa, z_{CO_2} = 0.674. Then, the second isopleth was measured. Results are gathered in table 4 and plots $x^L_{CO_2}$ against P are shown in Figure 7.

As observed in figure 7, the data represented seem to follow smooth tends and describe well the dependence of solubility with pressure and temperature. As the device operated continuously during measurement of all points, and isopleths are determined faster than isotherms, the experimental time required to measure this system was significantly lower than for previous. Moreover, isopleth plots are much less scattered, which is reasonable taking into account that the uncertainty due to CO_2 loading is avoided.

The open points in figure 7 are experimentally determined data that should not correspond to thermodynamically stable states, as the temperature is much lower than the melting point under CO_2 atmosphere determined by Lopes et al.[13] However, they follow the same tendency as those at higher temperature, instead of a discontinuity expected upon solidification. This is because, once it has melted, the IL remains in liquid state at every temperature, a fact that was confirmed visually at the end of each experiment. This had been

previously observed: addition of CO_2 and other cosolvents to [Bmim][Cl] allowed to increase the liquid window of the latter; therefore, reactions can be carried out in it,[32] presumably, thanks to the formation of a metastable state.[33] During an experiment in our laboratory [Amim][Cl] under ~3 MPa of CO_2, the IL was not solidified even when it was cooled with liquid nitrogen. Thus, the data obtained in this work for the lowest temperatures correspond to metastable equilibria.

Theoretical modelling.

Extended Henry's law correlation.

The extended Henry's law can be applied to ILs assuming that the vapour phase consists only of pure CO_2. It can be expressed as shown in eq. 2, as stated by Soriano et al.[23]

$$k_{\mathrm{H,CO_2}}(T,P)\cdot a_{\mathrm{CO_2}}\left(T,m_{\mathrm{CO_2}}\right)=f_{\mathrm{CO_2}}(T,P) \quad (2)$$

Where $k_{\mathrm{H,CO_2}}(T,P)$ is the Henry's constant of CO_2 in IL for every pressure and temperature, $a_{\mathrm{CO_2}}\left(T,m_{\mathrm{CO_2}}\right)$ the activity of CO_2 in the IL as a function of temperature and molality and $f_{\mathrm{CO_2}}(T,P)$ the fugacity of CO_2 in the vapour phase.

The extended Henry's constant can be expressed as:

$$k_{\mathrm{H,CO_2}}(T,P)=k_{\mathrm{H,CO_2}}(T)\cdot\exp\left(\frac{\bar{V}^{\infty}_{m,\mathrm{CO_2}}P}{RT}\right) \quad (3)$$

Where $k_{\mathrm{H,CO_2}}(T)$ in the Henry's constant at the limit of zero pressure and $\bar{V}^{\infty}_{m,\mathrm{CO_2}}$ the partial molar volume of CO_2 in IL at infinite dilution. Dependence of $\bar{V}^{\infty}_{m,\mathrm{CO_2}}$ with temperature can be described lineally as:

$$\bar{V}^{\infty}_{m,\mathrm{CO_2}}=c_0+c_1T \quad (4)$$

With c_0 and c_1 being fitting parameters. The activity of CO_2 can be expressed in terms of molality as:

$$a_{CO_2}(T, m_{CO_2}) = \frac{m_{CO_2}}{m^0}\gamma^*_{CO_2} \quad (5)$$

Where m_{CO_2} and m^0 are the solubility of CO_2 in IL expressed in molality and the reference concentration (1 mol kg^{-1}) respectively. $\gamma^*_{CO_2}$ is the molality scale activity coefficient of CO_2, which can be calculated from the virial expansion developed by Pitzer[34] as:

$$\ln \gamma^*_{CO_2} = 2\frac{m_{CO_2}}{m^0}\beta^{(0)} + 3\left(\frac{m_{CO_2}}{m^0}\right)^2\tau^{(0)} \quad (6)$$

Where $\beta^{(0)}$ and $\tau^{(0)}$ are parameters related to binary and ternary interactions between molecules of CO_2 and IL. The $f_{CO_2}(T, P)$ was calculated from the equation of state integrated in the program REFPROP.[29] The $k_{H,CO_2}(T)$ can be calculated from an extrapolation of the experimental solubility data of CO_2 in IL.

$$k_{H,CO_2}(T) = \lim_{P\to 0}\left[\frac{f_{CO_2}(T,P)}{m_{CO_2}/m^0}\right] \quad (7)$$

By plotting $f_{CO_2}/(m_{CO_2}/m^0)$ against pressure and fitting the data to a proper regression, the $k_{H,CO_2}(T)$ corresponds to the zero-intercept. However, this method is only valid for sets of data m_{CO_2} vs. *P* at constant temperature (isotherms). Moreover, extrapolation can only be done if an enough amount of accurate data is available at low pressures, since a small error in the determination of solubility can lead to large deviations in $f_{CO_2}/(m_{CO_2}/m^0)$ vs *P*.

To avoid this, and also to extend the method to any kind of datasets, we propose the following alternative empirical approach: All the solubility data P vs x_{CO_2} were fitted to the following surface:

$$P = (a_0 + a_1 T)x_{CO_2} + (b_0 + b_1 T)x_{CO_2}^2 \quad (8)$$

Where a_0, a_1, b_0, b_1 are fitting parameters. This step is equivalent to the linear fitting prior to direct extrapolation done in literature[23] at each temperature. In this case a simultaneous fitting to the three isotherms (and potentially any experimental dataset not necessarily an isotherm) is done instead. After fitting equation 8, it can be used to calculate x_{CO_2} and m_{CO_2} at $P = 0$ for every temperature, and then estimate $k_{H,CO_2}(T)$ using equation 7.

As stated above, this proposed procedure overcomes the difficulty of having a dispersion in $f_{CO_2}/(m_{CO_2}/m^0)$ vs. P plot at low pressures, as it can be appreciated in Figure 8: $f_{CO_2}/(m_{CO_2}/m^0)$ calculated using the experimental solubility (symbols) has a dispersion that makes impossible any accurate extrapolation. However, using the empirical equation 8 (lines), a zero intercept can be estimated more accurately, and what is more, one can assure an increasing dependence of $k_{H,CO_2}(T)$ with temperature. Notice that this procedure is not restricted to isotherms but it can also be applied to isopleths and even to datasets with not specific sequence.

Once $k_{H,CO_2}(T)$ is determined, the model can be fitted by an iterative algorithm minimizing the average absolute relative deviation (AARD) between the calculated and experimental solubility. In the present work, only the parameters c_0, c_1 and $\beta^{(0)}$ were necessary to describe the experimental data. All the fitting parameters of this model for the three systems studied in this work are gathered in Table 5.

For the system CO_2 + [Emim][DEP] isothermal datasets (313.15, 333.15, and 353.15 K) were used for the regression. In order to test the prediction capacity of the model, the isopleth dataset was predicted with the parameters obtained. Results are shown in figure 4. The agreement between the experimental and calculated solubilities is excellent for the fitted curves and reasonably good for the predicted ones. For the system CO_2 + [Amim][Cl], the two isotherms experimentally determined were fitted. The resulting correlation is excellent, as shown in figure 6.

For the system [Bmim][Cl], however, the data corresponding to the two isopleths was used to fit the model, and the isotherm at 353.15 K was predicted instead. Only the points corresponding to thermodynamic stable phase equilibrium states were considered in the fitting. Results are displayed in figure 7. The model has an excellent prediction capacity for the isotherm and for the metastable equilibrium states at temperatures close to those considered in the fitting (down to 333.15 K). At the lowest temperatures the agreement in not that good.

Figure 9 presents $k_{\mathrm{H,CO_2}}$ plotted against $1/T$ obtained for the three systems studied in this work. The Henry's constant of each IL decreases with temperature as expected and depict values that are typical of other ILs. For low temperatures the dependency of $\ln k_{\mathrm{H,CO_2}}(T)$ vs. $1/T$ of the systems with chloride based ILs gets stronger than that observed in other reports,[23] which may be a consequence of the less ability of the model to predict extrapolated values.

The Group Contribution Equation of State

The GC-EOS, originally developed by Skjold-Jørgensen,[27,35] is based on the Van der Waals partition function combined with the local composition principle. It can be expressed as the sum of two contributions to the residual Helmholtz free energy $(A)_{res}$: a repulsive (*rep*) and an attractive (*att*) term:

$$\left(\frac{A}{RT}\right)_{res} = \left(\frac{A}{RT}\right)_{rep} + \left(\frac{A}{RT}\right)_{att} \quad (9)$$

The repulsive term uses the expression developed by Mansoori and Leland[36] for hard spheres:

$$\left(\frac{A}{RT}\right)_{rep} = 3\left(\frac{\lambda_1\lambda_2}{\lambda_3}\right)(Y-1) + \left(\frac{\lambda_2^3}{\lambda_3^2}\right)(-Y + Y^2 - \ln Y) + n\ln Y \quad (10)$$

Where

$$\lambda_k = \sum_i^{NC} n_i d_i^k \quad (11)$$

$$Y = \left(1 - \frac{\pi\lambda_3}{6V}\right)^{-1} \quad (12)$$

being n_i the number of moles of component *i*, *V* the total volume, *NC* the total number of components in the mixture, and d_i the hard-sphere diameter per mole. d_i is a function of temperature:

$$d_i = 1.065655 d_{c,i}\left[1 - 0.12\exp\left(-\frac{2T_{c,i}}{3T}\right)\right] \quad (13)$$

Where $T_{c,i}$ is the critical temperature and $d_{c,i}$ is the critical hard-sphere diameter which is normally calculated from the critical parameters $T_{c,i}$ and $P_{c,i}$ or vapour pressures. However, none of these data are available for the ILs. In this work, T_c was estimated using the method of Valderrama[37] and the $d_{c,i}$ of phosphate-based ILs were calculated from the correlation developed by Espinosa et al.[38] for high molecular weight compounds adapted to ILs.[39,40]

$$\log(d_{c,i}) = 0.4152 + 0.4128\log(r_{vdW,i}) \quad (14)$$

Where r_{vdW} is the Van der Waals molecular volume of the compound, estimated by a simple linear relation with respect to the molar volume of the IL at 298 K (v_{298}).[41]

$$r_{vdW} = 0.039 \cdot v_{298}(\mathrm{cm^3 mol^{-1}}) \quad (15)$$

On the other hand, the d_c of chloride-based ILs were taken from a previous work.[13]

The attractive contribution of the residual Helmholtz free energy (A^{att}) is a group contribution version of a density-dependent NRTL model.[42] It is expressed as:

$$\left(\frac{A}{RT}\right)_{att} = -\left(\frac{z}{2}\right)\sum_{i=1}^{NC} n_i \sum_{j=1}^{NG} v_j^i q_j \frac{\sum_{k=1}^{NG} \theta_k \left(\frac{g_{kj}\tilde{q}\tau_{kj}}{RTV}\right)}{\sum_{l=1}^{NG} \theta_l \tau_{lj}} \quad (16)$$

$$\tau_{kj} = \exp\left(\frac{\alpha_{kj}\Delta g_{kj}\tilde{q}}{RTV}\right) \quad (17)$$

$$\Delta g_{kj} = g_{kj} - g_{jj} \quad (18)$$

Where, z is the coordination number set equal to 10; NG is the number of groups, v_j^i is the number of groups j in component i; q_j is the number of surface segments assigned to group j; θ_k is the surface fraction of group k; q is the total number of surface segments; g_{ij} is the attractive energy parameter for interactions between segments j and i; and α_{ij} is the corresponding non-randomness parameter.

The interactions between unlike segments are defined by equation 19:

$$g_{ji} = k_{ij}\sqrt{g_{ii}g_{jj}} \quad (19)$$

Where $k_{ij} = k_{ji}$ is a symmetrical binary interaction parameter. Both, the attractive energy, g_{ii} and the binary interaction parameter, k_{ij}, depend on temperature as:

$$g_{ii} = g_{ii}^*\left[1 + g_{ii}'\left(\frac{T}{T_i^*} - 1\right) + g_{ii}''\ln\left(\frac{T}{T_i^*}\right)\right] \quad (20)$$

$$k_{ij} = k_{ij}^*\left[1 + k_{ij}'\ln\left(\frac{2T}{T_i^* + T_j^*}\right)\right] \quad (21)$$

Where g_{ii}^{*} and k_{ij}^{*} are the attractive energy and binary interaction parameters at the arbitrary, but fixed, reference temperature T_i^{*} and $(T_i^{*} + T_j^{*})/2$, respectively.

To apply the GC-EOS it is necessary to divide the IL molecule into functional groups. Breure et al.[39] showed that the anion and part of the cation, except for its alkyl chain, should be kept together in a single electroneutral group. Therefore, by adding the CH_2, CH_3 or other functional groups to the side alkyl chain, any IL of the same family can be assembled.

Modelling of the Phosphate-based ILs.

In a previous publication, de Pablo et al. [43] correlated some GC-EOS parameters using infinite dilution activity coefficients of hydrocarbon in imidazolium and phosphate based IL. Pure parameters for the groups -mimDEP and -mimDMP and the corresponding binary interaction parameters with typical hydrocarbon groups were determined. In this work, that study is extended to CO_2 solubility data by correlating binary interaction parameters between groups -mimDEP or -mimDMP and CO_2. Thus the GC-EOS is applied to correlate and predict data for CO_2 solubility in 1-ethyl-3-methylimidazolium diethylphosphate, [Emim][DEP]; 1-ethyl-3-methylimidazolium dimethylphosphate, [Emim][DMP] and 1,3-dimethylimidazolium dimethylphosphate, [Dmim][DMP]) from this work and from the literature. The characteristic groups for Phosphate-based ILs,e -mimDMP and -mimDEP, are shown in Figure 10. Table 6 gathers the parameters for the IL studied in this work.

Table 7 summarizes the experimental database used. Solubility data for the system CO_2 + [Emim][DEP] from Ramdin et al.[15] and those obtained in this work along with another

dataset for the system CO_2 + [Dmim][DMP] determined by Palgunadi et al.[20] were used for correlation. Data for CO_2 solubility in [Emim][DEP] at lower pressure[20] was chosen for ensuring its prediction ability. The data from Mejía et al.[19] were not included due to the high uncertainty of the experimental data; the authors conclude that not including them would improve the overall quality of the correlation.

Table 8 gathers the pure group energy parameters: $g_{ii}^{*}, g_{ii}', g_{ii}''$, the surface area q_i, and the reference temperature T_i* obtained from the literature. Binary interaction parameters are displayed in Table 9. They were obtained from literature except those between the groups -mimDMP and CO_2 and -mimDEP$^-$that were calculated from the correlation with the experimental datasets in Table 7.

As seen in Table 7 and figure 4 the GC-EOS model can describe very well the experimental data measured in this work. Accuracy at 313.15 K, however, was a bit lower than at higher temperatures. The model is even able to describe the isopleth at nearly every temperature much better than the Extended Henry's Law model. The model also succeeded at correlating the literature data. For the system CO_2 + [Dmim][DMP] the agreement is excellent. Calculation of solubility data at low pressures for the system CO_2 + [Emim][DEP] resulted in values with a medium accuracy (relative deviation of 21%) respect the experimental data. Providing it is a prediction and the GC-EOS has a limitation at low CO_2 concentration, the results are acceptable.

Modelling of the chloride-based ILs

GC-EOS is used also for the correlation of CO_2 equilibrium of methyl imidazolium chloride based ILs, as [Bmim][Cl] and [Amim][Cl]. Lopes et al.[13] correlated data from Jang

et al.[44] for the system CO_2 + [Bmim][Cl] to obtain the interaction parameters. between groups -mimCl and CO_2. Nonetheless, the experimental data reported by Jang et al. deviates largely with respect the values obtained in this work and reported in Section 3.3. This discrepancy is illustrated in Figure 11 for the system CO_2 + [Bmim][Cl] at 353.15 K, where it is clear that the data reported by Jang et al. depicts a much larger solubility of CO_2 in [Bmim][Cl] that the one presented here. Since the discrepancy between these datasets is significant, we have recalculated such parameters using the experimental data obtained in this work. As in the previous case, the modelling starts by the definition of the groups. Following Lopes et al. [13] recommendation the ILs [Bmim][Cl] and [Amim][Cl] were fractionated as shown in Figure 12. Table 10 gathers the parameters for the chloride-based ILs studied in this work. Moreover, Table 11 summarizes the database used for the correlation.

Table 8 presents the pure group parameters: $g_{ii}^{*}, g_{ii}', g_{ii}''$, the surface area q_i, and the reference temperature T_i* used is this work, and Table 9 lists the binary interaction parameters obtained from literature and the ones correlated in this work. It is worth noticing that the only parameters that have been refitted are the interaction parameters between CO_2 and -mimCl groups.

Figure 7 shows an excellent correlation for the data of CO_2 solubility in [Bmim][Cl] with an ARD of only 3.5 %. The model is able to describe both the isotherm and the two isopleths for all the temperature range. The model, however, fails to predict with the same accuracy the data for the system CO_2 + [Amim][Cl], achieving an ARD of 15% and 31% for the 333.15 and 353 K isotherms. As seen in Fig. 6, the predicted isotherms fall in the

middle of the experimental data; therefore, an improvement of one isotherm could affect the other. Furthermore, although the GC-EOS predicts this system with a lower quality than the Extended Henry's Law model, it should be taken into account that the results of the GC-EOS for CO_2 + [Amim][Cl] are completely predicted by group-contribution, since no information of this system was used in the parameterization. Consequently, the results obtained with the GC-EOS are still satisfactory.

Conclusions

CO_2 solubility in [Emim][DEP], [Amim][Cl] and [Bmim][Cl] at temperatures between 298 and 356 K and pressures up to 6.5 MPa were determined using a static isochoric method. The versatility of the device can be improved by considering that it can be operated in either isothermal or isoplethal mode. A detailed analysis of uncertainties revealed that the larger contributions to the overall uncertainty were the calibration of the cell volume, the density of the liquid phase, and the addition of CO_2. The latter, however, was much lower during an isopleth measurement. A two-parameter extended Henry's law correlation was used to represent the experimental data with excellent results, but a previous empirical fitting step had to be introduced to minimize uncertainties of the Henry's constant at the limit of zero pressure. The data were also correlated with the Group Contribution Equation of State with satisfactory results. New binary parameters between CO_2 and -mimDEP, -mimDMP and –mimCl were correlated. Excellent results were obtained for all CO_2 + IL systems, except for that with [Amim][Cl], which is rather qualitative.

Aknowledgments

The work was funded by the MINECO through the project ENE2014-53459-R and Junta de Castilla y León through the project VA248P18. LP thanks the Erasmus Mundus Eurica PhD student grant for the economic support. MDB thanks the Spanish Ministry of Economy and Competitiveness for the Ramón y Cajal research fellowship. FAS and SP also acknowledge the financial support granted by the Consejo Nacional de Investigaciones Científicas y Técnicas (PIP 112 2015 010 856), the Ministerio de Ciencia, Tecnología e Innovación Productiva (PICT 2016 0907), and Universidad Nacional del Sur (PGI - 24/M133).

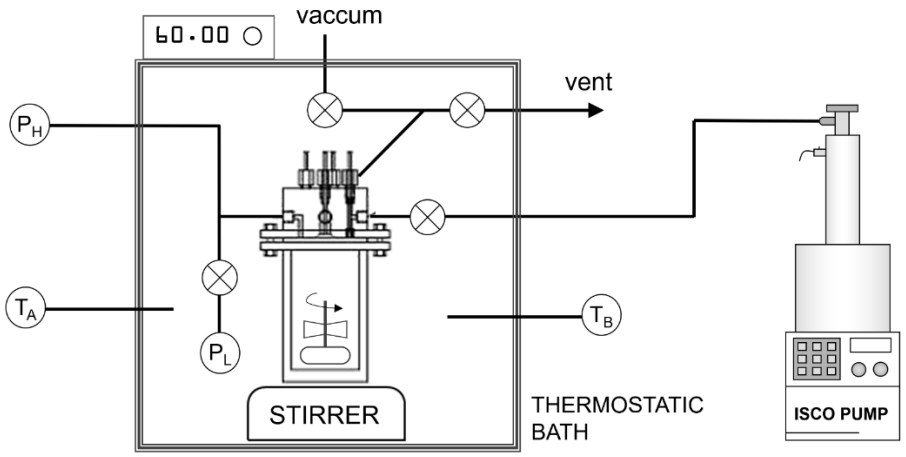

Figure 1. Experimental equipment used for the determination of CO_2 solubilities in IL P_L and P_H are the transducers for low and high pressure range. T_A and T_B are two duplicated measurements of the temperature of the bath.

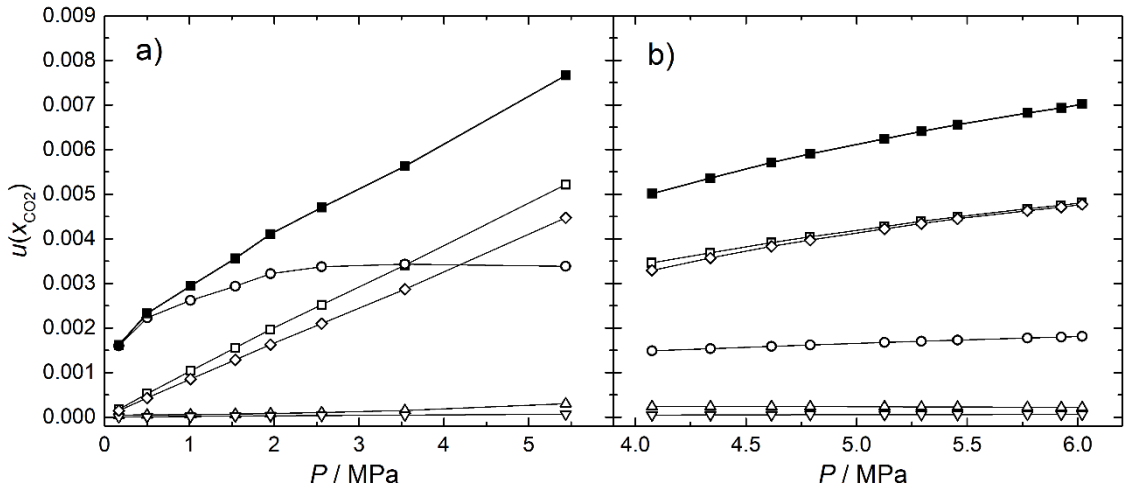

Figure 2. Contributions of each variable to the total uncertainty for the solubility measurements. Calculated for the system CO_2 + [Emim][DEP] along a) an isotherm at T = 333.15 K. b) an isopleth at x_{CO_2} = 0.751. Contribution of (—○—): CO_2 addition, (—□—): calibration, (—◇—): density of the liquid phase, (—△—): density of the gas phase, (—▽—): IL addition. (—■—): Total uncertainty.

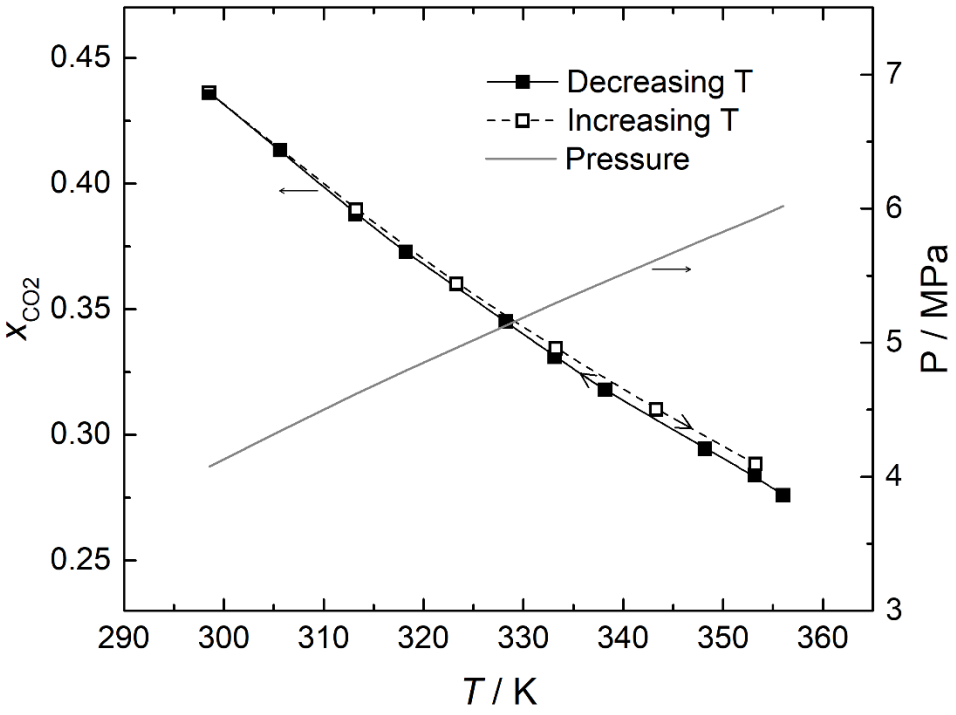

Figure 3. Hysteresis evaluation for the measurement of CO_2 solubility in [Emim][DEP] along an isotherm at the overall concentration of z_{CO_2} = 0.674 upon increasing and decreasing temperature.

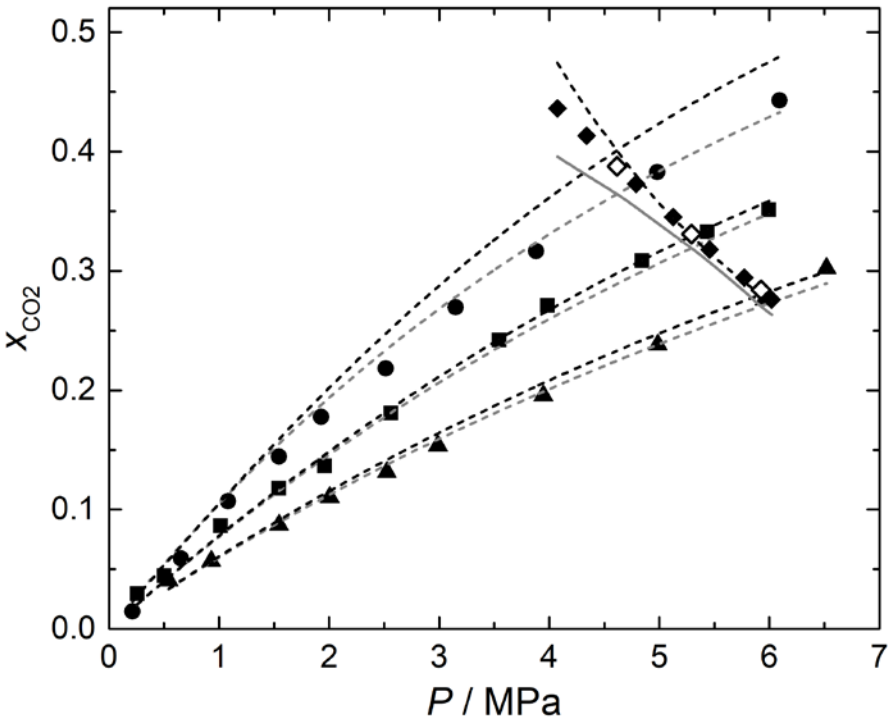

Figure 4. Experimental solubilities for the system CO_2 + [Emim][DEP] at (●): 313.15 K, (■): 333.15, (▲): 353.15 K. (◆): Isopleth measured at z_{CO_2} = 0.751. The open symbols are those belonging to the isopleth determined at 313.15, 333.15 and 353.5 K, which are in agreement to the isotherms. Calculated solubilities with (**grey lines**): Extended Henry's law correlation; (**black lines**): GC-EOS. In both cases, dotted lines are correlations and solid lines are predictions.

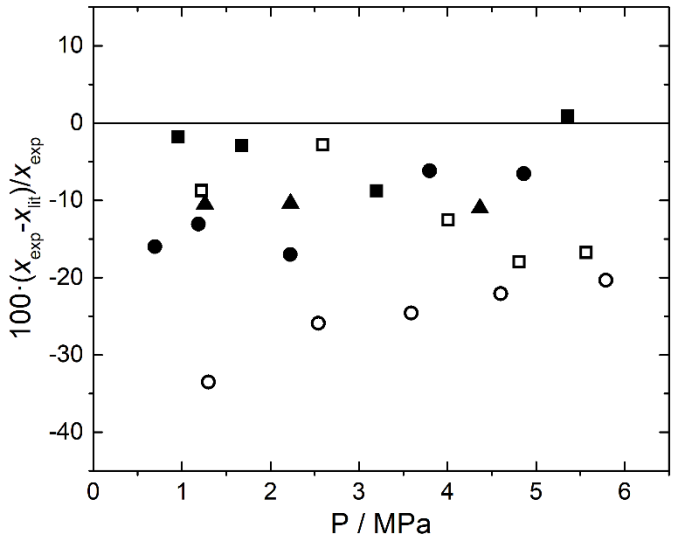

Figure 5. Experimental deviations for the solubility of CO_2 in [Emim][DEP] between data obtained in this work and in literature: (●): 313.15 K, (■): 333.15, (▲):353.15 K. Closed symbols are data by Ramdin et al.[16] and open symbols are for data by Mejía et al.[19]

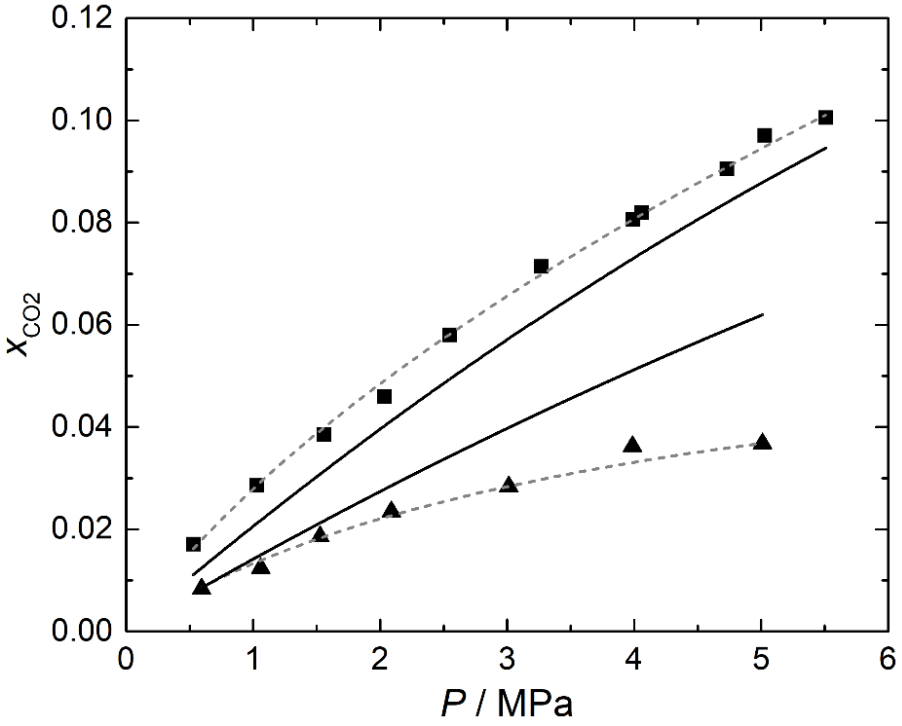

Figure 6. Experimental solubilities for the system CO_2 + [Amim][Cl] at (■): 333.15, (▲): 353.15 K. Calculated solubilities with (**grey lines**): Extended Henry's law correlation; (**black lines**): GC-EOS. In both cases, dotted lines are correlations and solid lines are predictions.

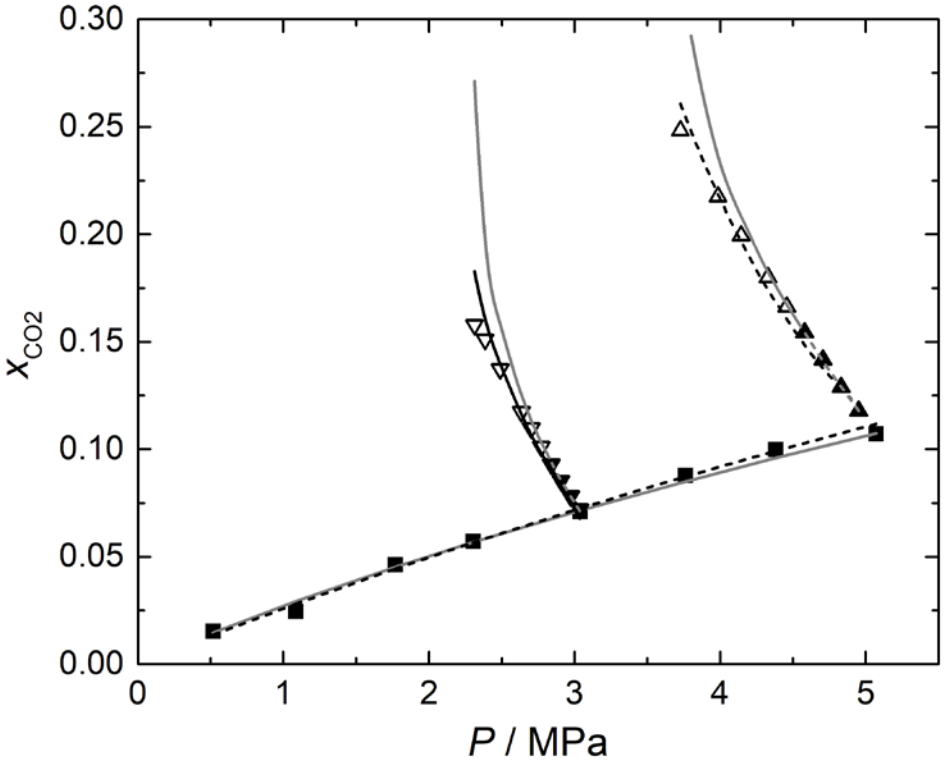

Figure 7. Experimental solubilities for the system CO_2 + [Bmim][Cl]. (■): Isotherm at 353.15 K. (▼): Isopleth at z_{CO_2} = 0.538. (▲): Isopleth at z_{CO_2} = 0.674. The open symbols correspond to data experimentally determined at a metastable equilibrium. Calculated solubilities with (**grey lines**): Extended Henry's law correlation; (**black lines**): GC-EOS. In both cases, dotted lines are correlations and solid lines are predictions.

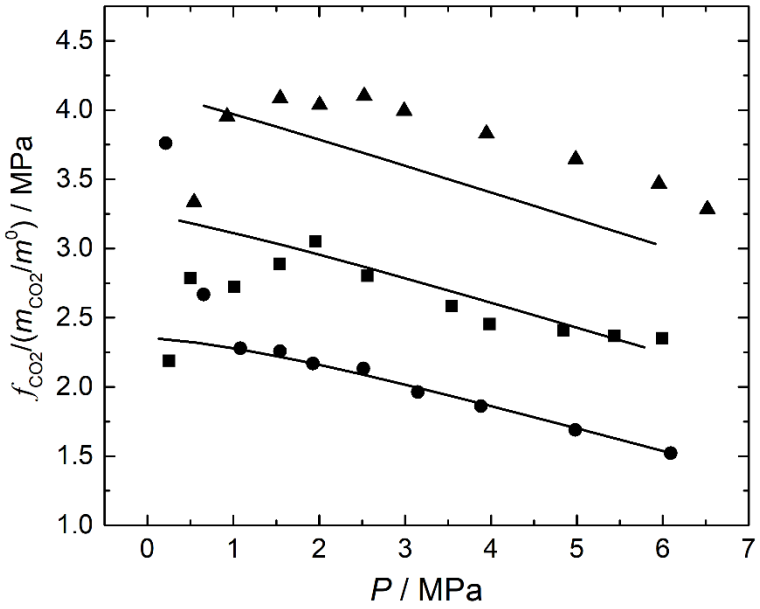

Figure 8. Plot of $f_{CO_2}/(m_{CO_2}/m^0)$ vs. P for the system CO_2 + [Emim][DEP] at (●): 313.15 K, (■): 333.15, (▲): 353.15 K. Lines are the corresponding values calculated from fitting equation 8 to experimental data.

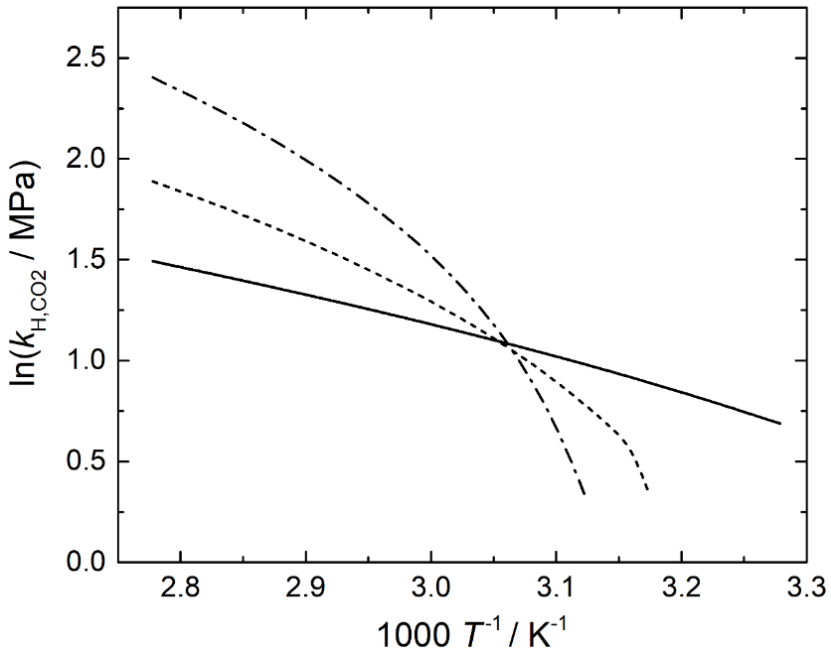

Figure 9. Henry's constant of CO_2 at zero pressure in the studied ILs versus 1/T. (——): [Emim][DEP]. (–·–·–): [Amim][Cl]. (------): [Bmim][Cl]

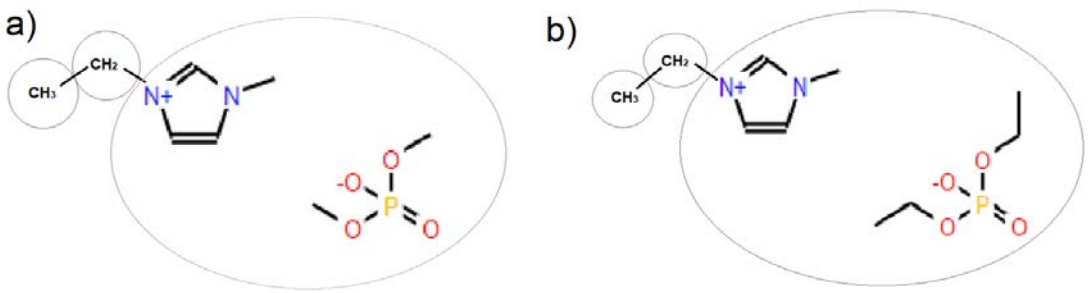

Figure 10. Group definition for a) -mimDMP and b) –mimDEP.

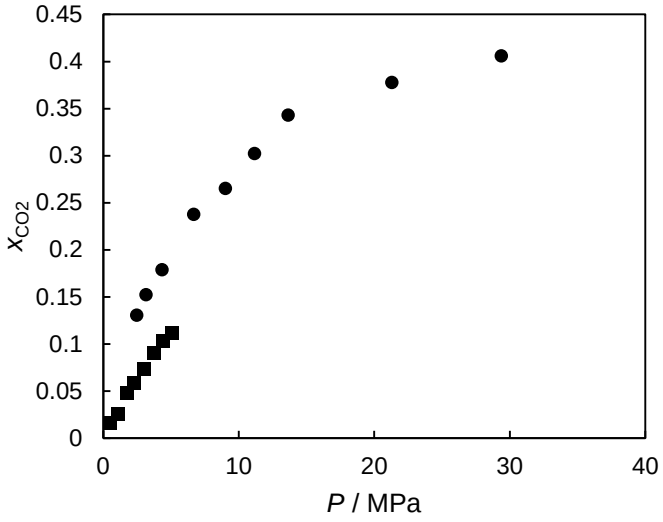

Figure 11. Comparison between experimental data from Jang et al.[44] (●) and data measured in this work (■), both sets of data corresponding to the binary system [Bmim][Cl] + CO_2 at 353.15 K

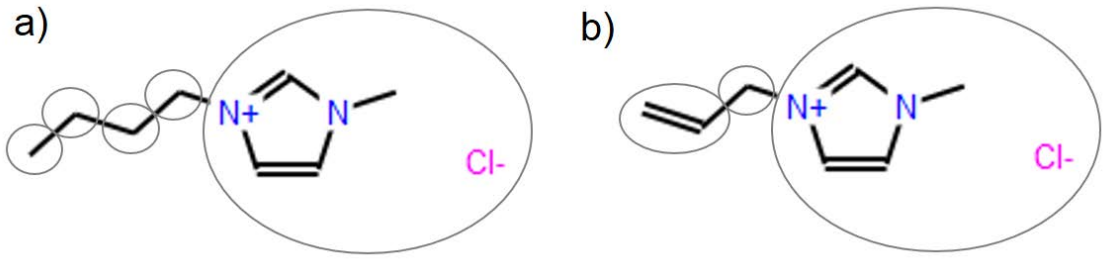

Figure 12. Group definition for -mimCl in a) [Bmim][Cl] and b) [Amim][Cl].

Table 1. Contributions to uncertainty for the measurement of CO_2 solubility in IL.

Source of uncertainty	**Value**
• IL Loading	$u(w_{IL})$ = 0.005 g
• Addition of CO_2	$u(w)$ = 0.0095 g (each addition)
Pump temperature.	$u(T_{pump})$ = 0.1 K
Pump pressure	$u(P_{pump})$ = 0.005 MPa
Density of CO_2 added	$u(\rho_{add})$ = 0.63 kg m^{-3}
Volume added	$u(V_{add})$ = 0.01 mL
• Calibration of the cell volume	$u(V)$ = 0.39 mL
• Density of the liquid phase	$u(\rho^L) / \rho^L$ = 0.01
• Density of the gas phase (CO_2)	$u(\rho_{CO2}) / \rho_{CO2}$ = 0.001 – 0.006 (within an interval of 0.17 – 5.4 MPa)
Cell temperature	$u(T)$ = 0.02 K
Cell pressure	$u(P) / P = 10^{-4}$

Table 2. Experimental solubilities for the system CO_2 + [Emim][DEP].

Isotherm, T = 313.15 K					
P / MPa	$x^L_{CO_2}$	P / MPa	$x^L_{CO_2}$	P / MPa	$x^L_{CO_2}$
0.2142	0.015	1.9282	0.178	3.8821	0.317
0.6536	0.059	2.5155	0.218	4.9806	0.383
1.0818	0.107	3.1491	0.269	6.0922	0.443
1.5429	0.145				
Isotherm, T = 333.15 K					
P / MPa	$x^L_{CO_2}$	P / MPa	$x^L_{CO_2}$	P / MPa	$x^L_{CO_2}$
0.2547	0.030	1.9563	0.137	4.8433	0.308

0.5010	0.045	2.5602	0.181	5.4380	0.333
1.0138	0.087	3.5424	0.242	5.9967	0.351
1.5412	0.118	3.9828	0.271		

Isotherm, T = 353.15 K

P / MPa	$x^L_{CO_2}$	P / MPa	$x^L_{CO_2}$	P / MPa	$x^L_{CO_2}$
0.5431	0.041	2.5250	0.131	4.9855	0.238
0.9286	0.057	2.9900	0.154	5.9560	0.276
1.5454	0.087	3.9475	0.196	6.5200	0.302
2.0059	0.110				

Isopleth, z_{CO_2} = 0.751

T / K	P / MPa	$x^L_{CO_2}$	T / K	P / MPa	$x^L_{CO_2}$
356.02	6.0195	0.276	328.23	5.1268	0.345
353.18	5.9251	0.284	318.22	4.7902	0.373
348.17	5.7720	0.294	313.16	4.6155	0.388
338.18	5.4564	0.318	305.65	4.3393	0.413
333.15	5.2927	0.331	298.55	4.0752	0.436

u(P)/P = 2×10^{-4} and 10^{-4} for P < 2 MPa and P > 2 MPa respectively.

Table 3. Experimental solubilities for the system CO_2 + [Amim][Cl].

Isotherm, T = 333.15 K

P / MPa	$x^L_{CO_2}$	P / MPa	$x^L_{CO_2}$	P / MPa	$x^L_{CO_2}$
0.5300	0.017	2.5502	0.058	4.7321	0.090
1.0300	0.029	3.2692	0.071	5.0304	0.097
1.5610	0.039	3.9935	0.081	5.5081	0.101

2.0358	0.046	4.0612	0.082		

Isotherm, T = 353.15 K

P / MPa	$x^L_{CO_2}$	P / MPa	$x^L_{CO_2}$	P / MPa	$x^L_{CO_2}$
0.5931	0.008	2.0896	0.023	3.9879	0.036
1.0606	0.012	3.0141	0.028	5.0106	0.037
1.5260	0.019				

u(P)/P = 2×10^{-4} and 10^{-4} for P < 2 MPa and P > 2 MPa respectively.

Table 4. Experimental solubilities for the system CO_2 + [Bmim][Cl].

Isotherm, T = 353.15 K

P / MPa	$x^L_{CO_2}$	P / MPa	$x^L_{CO_2}$	P / MPa	$x^L_{CO_2}$
0.5176	0.0153	2.3035	0.0571	4.3832	0.0999
1.0850	0.0246	3.0387	0.0710	5.0717	0.1072
1.7680	0.0463	3.7615	0.0878		

Isopleth, z_{CO_2} = 0.538

T / K	P / MPa	$x^L_{CO_2}$	T / K	P / MPa	$x^L_{CO_2}$
353.15	3.0364	0.072	328.11	2.7018	0.110
348.10	2.9727	0.078	323.14	2.6350	0.117
343.12	2.9072	0.085	313.15	2.4887	0.137
338.12	2.8403	0.093	305.95	2.3852	0.151
333.14	2.7719	0.101	299.97	2.3123	0.158

Isopleth, z_{CO_2} = 0.674

T / K	P / MPa	$x^L_{CO_2}$	T / K	P / MPa	$x^L_{CO_2}$
348.11	4.9516	0.118	323.15	4.3288	0.180
343.12	4.8310	0.129	315.97	4.1445	0.199
338.14	4.7063	0.142	309.97	3.9852	0.218

333.15	4.5812	0.154	300.49	3.7273	0.248
328.14	4.4573	0.166			

u(P)/P = 2×10^{-4} and 10^{-4} for P < 2 MPa and P > 2 MPa respectively.

Table 5. Fitted parameters and AARD for the correlation of the experimental solubility of CO_2 in the ILs studied in this work with equation 8 and the extended Henry's law.

	CO_2 + [Emim][DEP]	**CO_2 + [Amim][Cl]**	**CO_2 + [Bmim][Cl]**
Polynomial Surface (equation 8)			
a_0 /MPa	-44.05	-480.9	-191.1
b_0 /MPa	-4.118	-18936	-861.6
a_1 / MPa K^{-1}	0.1691	1.529	0.6358
b_1 / MPa K^{-1}	0.0481	57.62	2.760
AARD%	8.0	4.0	2.5
Extended Henry's law correlation			
c_0 / m^3 mol^{-1}	-2474.3	-6414.0	-2981.8
c_1 / m^3 mol^{-1} K^{-1}	6.1746	18.3360	7.8524
$\beta^{(0)}$	0.3085	0.9757	0.5107
AARD% (fit)	6.2	3.2	4.0
AARD% (prediction)	8.1	-	21.2[a]
			4.4[b]

[a] for the points in metastable equilibrium

[b] for the isotherm

Table 6. Molar volumes at 298 K, van der Waals volume, and critical diameter for the imidazolium alkylphaphate-based ionic liquids studied in this work.

Ionic Liquid	v_{298} / $cm^3 \cdot mol^{-1}$	Source	r_{vdW} / $cm^3 \cdot mol^{-1}$	d_c / $cm \cdot mol^{-1/3}$	T_c /K
[Emim][DEP]	230.57	[45]	8.992	6.4432	789.0
EmimDMP	194.10	[46]	7.570	6.0000	748.6
[Dmim][DMP]	176.57	[47]	6.886	5.7671	869.4

Table 7. Database of solubility of CO_2 in the different phosphate-based ionic liquids used in this work

Compound / Ionic liquid	T /K	P /MPa	Data uncertainty	No exp. Points	ARD% (x_{CO2})	Source
[Emim][DEP]*	313.15–353.15	0.075–6.0	±2%	45	7.2	This work
[Emim][DEP]*	302.69–362.13	0.534–10.948	8%–11%	35	6.4	[15]
[Emim][DEP]	313.15–333.15	0.023–0.193	0.7%–4%	22	21	[20]
[Dmim][DMP]*	313.15–333.15	0.048–0.170	0.7%–2%	12	2.6	[20]

* Data used for the correlation

Table 8. GC-EOS pure group parameters. T_i* is the reference temperature, q_i is the surface area of *i* and *g**, *g*', and *g*'' are the pure group energy parameters and their temperature dependence.

Group	T^* / K	q	g^* / atm·cm^6·mol^{-2}	g'	g''	Source
-mimDMP	600	4.8513	1154081	-0.2941	0	[43]
-mimDEP	600	6.0116	1170489	-0.1153	0	[43]
-mimCl	600	2.855	1844397	-0.1552	0	[13]
CH_3	600	0.848	316910	-0.9274	0	[48]
CH_2	600	0.540	356080	-0.8755	0	[48]
CH_2=CH	600	1.176	337980	-0.6764	0	[48]
CO_2	308.2	1.261	531890	-0.578	0	[48]

Table 9. GC-EOS binary interaction parameters obtained from literature and correlated in this work.

Group i	Group j	k_{ij}^*	k_{ij}'	α_{ij}	α_{ji}	Source
-mimDMP	CH_3	1.0169	-0.0477	-1.868	-3.1969	[43]
	CH_2	1.0169	-0.0477	-2.3677	-1.1145	[43]
	CO_2	1.1044	0	-5.0422	-1.6967	This work
-mimDEP	CH_3	0.999	-0.0084	8.7504	-1.8958	[43]
	CH_2	0.999	-0.0084	1.3137	-1.0597	[43]
	CO_2	1.1159	0	-9.1299	4.2409	This work
-mimCl	CH_3	0.8215	0	-0.7577	-0.2539	[13]
	CH_2	1.0271	0.0630	-0.7577	-0.2539	[13]

	CH_2=CH	0.7850	0	0	0	[13]
	CO_2	0.8534	-0.1733	0	0	This work
CH_3	CH_2	1	0	0	0	[48]
	CO_2	0.892	0	3.3690	3.3690	[48]
	CH_2=CH-	1	0	0	0	[48]
CH_2	CO_2	0.814	0	3.3690	3.3690	[48]
	CH_2=CH-	1	0	0	0	[48]
CH_2=CH-	CO_2	0.9480	0	0	0	[48]

Table 10. Van der Waals volume, critical diameter, and critical temperature for the imidazolium chloride-based ILs studied in this work.

Ionic Liquid	Source	r_{vdW} / $cm^3 \cdot mol^{-1}$	d_c / $cm \cdot mol^{-1/3}$	T_c /K
[Bmim][Cl]	13	6.7513	5.7223	789.0
[Amim][Cl]	13	5.8470	5.3925	770.7

Table 11. Database of solubility of CO_2 in imidazolium chloride-based ionic liquids.

Compound	T /K	P /MPa	Data uncertainty	No exp.	Source

Ionic liquid				Points	ARD% (x_{CO2})	
[Bmim][Cl]*	299.97–353.15	.5–4.8	±2%	27	3.5	This work
[Amim][Cl]	333.15–353.15	.5–5.4	±2%	18	21	This work

* Data used for the correlation, except one isopleth used for the prediction.

References

1 Brennecke JF, Maginn EJ. Ionic liquids: Innovative fluids for chemical processing. AIChE J. 2001;47: 2384-2389.

2 Brandt A, Grasvik J, Hallett JP, Welton T. Deconstruction of lignocellulosic biomass with ionic liquids. Green Chem. 2013;15:550-583.

3 Vitz J, Erdmenger T, Schubert US. Imidazolium based ionic liquids as solvents for cellulose chemistry. In: Liebert TF, Heinze TJ, Edgar KJ. Cellulose solvents: For analysis, shaping and chemical modification. Washington DC:ACS Symposium Series, 2010:299-317.

[4] Mukherjee A, Mandal T,Ganguly A, Chatterjee PK. Lignin degradation in the production of bioethanol - A review. ChemBioEng Rev. 2016;3:86-96.

[5] Jaworska MM, Gorak A. New ionic liquids for modification of chitin particles. Mater Lett. 2016;164: 341-343.

6 Ohno H, Fukaya Y. Task specific ionic liquids for cellulose technology. Chem Lett. 2009;38:2-7.

7 Scheibel JJ, Kenneally CJ, Menkaus JA, Seddon KR, Chwala P. Methods for modifying cellulosic polymers in ionic liquids. 2007. Patent US20070225190A1.

[8] Lopes JM, Bermejo MD, Pérez E, Martín A, Segovia Puras JJ, Cocero MJ. Effect of $scCO_2$ on the kinetics of acetylation of cellulose using 1-allyl-3-methylimidazolium chloride as solvent. Experimental study and modeling. 2018;141:97-103.

9 Cao Y, Wu J, Meng T, Zhang J, He J, Li H, Zhang Y. Acetone-soluble cellulose acetates prepared by one-step homogeneous acetylation of cornhusk cellulose in an ionic liquid 1-allyl-3-methylimidazolium chloride (AmimCl), Carbohydr Polym. 2007;69:665–672.

[10] Blanchard LA, Brennecke JF. Recovery of organic products from ionic liquids using supercritical carbon dioxide. Ind Eng Chem Res. 2001;40:287-292.

11 Lopes JM, Kareth S, Bermejo MD, Martín A, Weidner E, Cocero MJ. Experimental determination of viscosities and densities of mixtures carbon dioxide + 1-allyl-3-methylimidazolium chloride. Viscosity correlation. J Supercrit Fluids. 2016;111:91 – 96.

[12] Tomida D, Kenmochi S, Quiao K, Bao Q, Yokoyama C. Viscosity of 1-buthyl-3-methylimidazolium hexafluorophosphate + CO_2. Fluid Phase Equilib. 2011;207:185-189.

[13] Lopes JM, Sánchez FA, Reartes SBR, Bermejo MD, Martín A, Cocero MJ. Melting point depression effect with CO_2 in high melting temperature cellulose dissolving ionic liquids. Modeling with group contribution equation of state. J Supercrit Fluids. 2016;107:590-604.

[14] Kazarian SJ, Sakellarios N, Gordon CM, High pressure CO_2-induced reduction of the melting temperatura of ionic liquids, Chem Commun. 2002:1314-1315.

[15] Kühne E, Pérez E, Witkamp GJ, Peters CJ. Solute influence on the high-pressure phase equilibrium of ternary systems with carbon dioxide and an ionic liquid. J Supercrit Fluids. 2008;45:27–31.

16 Ramdin M, Amplianitis A, Bazhenov S, Volkov A, Volkov V, Vlugt TJHH, de Loos TW. Solubility of CO_2 and CH_4 in ionic liquids: Ideal CO_2/CH_4 selectivity. Ind Eng Chem Res. 2014;53:15427-15435.

17 Jang S, Cho D-W, Im T, Kim H. High-pressure phase behavior of CO_2 + 1-butyl-3-methylimidazolium chloride system. Fluid Phase Equilib. 2010;299:216–221.

[18] Carvalho PJ, Álvarez VH, Marrucho IM, Aznar M, Coutinho JAP. High pressure phase behavior of carbon dioxide in 1-butyl-3-methylimidazolium bis(trifluoromethylsulfonyl)imide and 1-butyl-3-methylimidazolium dicyanamide ionic liquids. J. Supercrit Fluids. 2009;50:105–111.

19 Mejía I, Stanley K, Canales R, Brennecke JF. On the high-pressure solubilities of carbon dioxide in several ionic liquids. J Chem Eng Data. 2013;58:2642-2653.

20 Palgunadi J, Kang JE, Nguyen DQ, Kim JH, Min BK, Lee SD, Kim H, Kim HS. Solubility of CO_2 in dialkylimidazolium dialkylphosphate ionic liquids. Thermochim Acta. 2009;494:94-98.

[21] Kim YS, Jang JH, Lim BD, Kang JW, Lee CS. Solubility of mixed gases containing carbon dioxide in ionic liquids: Measurements and predictions. Fluid Phase Equilib. 2007;256:70–74.

[22] Zhou L, Fan J, Shang X, Wang J. Solubilities of CO_2, H_2, N_2 and O_2 in ionic liquid 1-n-butyl-3-methylimidazolium heptafluorobutyrate. J Chem Thermodyn. 2013;59:28–34.

[23] Soriano AN, Doma Jr. BT, Li M-H. Carbon dioxide solubility in some ionic liquids at moderate pressures. J Taiwan Inst Chem Eng. 2009;40:387-393.

[24] Shiflett MB, Yokozeki A. Solubilities and diffusivities of carbon dioxide in ionic liquids: [bmim][PF_6] and [bmim][BF_4]. Ind Eng Chem Res. 2005;44:4453-4464.

[25] Nonthanasin T, Henni A, Saiwan C. Densities and low pressure solubilities of carbon dioxide in five promising ionic liquids. RSC Adv. 2014;4:7566–7578.

[26] Zakrzewska ME, Rosatella AA, Simeonov SP, Afonso CAM, Najdanovic-Visak V, da Ponte MN. Solubility of carbon dioxide in ammonium based CO_2-induced ionic liquids. Fluid Phase Equilib. 2013;354:19–23.

27 Skjold-Jørgensen S, Group contribution equation of state (GC-EOS): a predictive method for phase equilibrium computations over wide ranges of temperature and pressures up to 30 MPa. Ind Eng Chem Res. 1988;53:15427-15435.

28 Gibbs RE, Van Ness HC, Vapor-liquid equilibria from total-pressure measurements. A new apparatus. Ind Eng Chem Fund. 1972;11:410-413.

[29] Lemmon EW, Span R. Short fundamental equations of state for 20 industrial fluids. J. Chem. Eng. Data. 2006;51:785-850.

30 Machida H, Taguchi R, Sato Y, Smith Jr. RL. Measurement and correlation of high pressure densities of ionic liquids, 1-ethyl-3-methylimidazolium l-lactate ([emim][Lactate]), 2-hydroxyethyl-trimethylammonium l-lactate ([$(C_2H_4OH)(CH_3)_3N$][Lactate]), and 1-butyl-3-methylimidazolium chloride ([bmim][Cl]). J Chem Eng Data. 2011; 56: 923–928.

31 Pérez E, Cabañas A, Sánchez-Vicente Y, Renuncio JAR, Pando C. High-pressure phase equilibria for the binary system carbon dioxide + dibenzofuran. J Supercrit Fluids. 2008;46:238-244.

[32] Qi X, Watanabe M, Aida TM, Smith Jr. RL. Efficient catalytic conversion of fructose into 5-hydroxymethylfurfural in ionic liquids at room temperature. ChemSusChem. 2009;2:944 – 946.

33 Smith Jr. RL, Fang Z. Properties and phase equilibria of fluid mixtures as the basis for developing green chemical processes. Fluid Phase Equilib. 2011;302:65–73.

[34] Pitzer KS. Thermodynamics of electrolytes. 1. Theoretical basis and general equations. J Phys Chem A. 1973;77:268-277.

35 Skjold-Jørgensen S. Gas solubility calculations. II. Application of a new group-contribution equation of state. Fluid Phase Equilib. 1984;16:317-351.

36 Mansoori GA, Carnahan NF, Starling KE, Leland TW. Equilibrium thermodynamic properties of the mixture of hard spheres, J Chem Phys. 1971;54:1523-1525.

[37] Valderrama JO, Rojas RE. Critical properties of ionic liquids. Revisited. Ind Eng Chem Res. 2009;48: 6890-6900.

38 Espinosa S, Fornari T, Bottini SB, Brignole EA, Phase equilibria in mixtures of fatty oils and derivatives with near critical fluids using the GC-EOS model, J Supercrit Fluids. 2002;23:91-102.

39 Breure B, Bottini SB, Witkamp G, Peters CJ, Thermodynamic modeling of the phase behavior of binary systems of ionic liquids and carbon dioxide with the group contribution equation of state, J Phys Chem B. 2007;111:14265-14270.

40 Bermejo MD, Martin A, Foco G, Cocero MJ, Bottini SB, Peters CJ, Application of a group contribution equation of state for the thermodynamic modeling of the binary systems CO_2-1-butyl-3-methyl imidazolium nitrate and CO_2-1-hydroxy-1-propyl-3-methyl imidazolium nitrate, J Supercrit Fluids. 2009;50:112-117.

41 Pereda S, Raeissi S, Andreatta AE, Bottini SB, Kroon M, Peters CJ, Modeling gas solubilities in imidazolium based ionic liquids with the [Tf_2N] anion using the GC-EoS. Fluid Phase Equilib. 2016;409:408-416.

42 Renon H, Prausnitz JM, Local compositions in thermodynamics excess functions for liquids mixtures, AIChE J. 1968;14:116-128.

43 Nisa LP, Sanchez FA, Bermejo MD, Pereda S. GC-EoS extension to alkylphosphate imidazolium ionic liquids. Fluid Phase Equilib. 2019;479:25-32.

[44] Jang J, Cho DWW, Im T, Kim H, High-pressure phase behavior of CO_2+1-butyl-3-methylimidazolium chloride system, Fluid Phase Equilib. 2010;299:216–221.

45 Cai F, Ibrahim JJ, Gao L, Wei R, Xiao GA. A study on the liquid-liquid equilibrium of 1-alkyl-3-methylimidazolium dialkylphosphate with methanol and dimethyl carbonate. Fluid Phase Equilib. 2014;382:254-259.

46 Freire MG, Teles ARR, Rocha MAA, Schröder B, Neves CMSS, Carvalho PJ, Evtuguin DV, Santos LMNBF, Coutinho JAP. Thermophysical characterization of ionic liquids able to dissolve biomass. J Chem Eng Data. 2011;56:4813-4822.

47 Wang J, Li C, Shen C, Wang Z. Towards understanding the effect of electrostatic interactions on the density of ionic liquids. Fluid Phase Equilib. 2014;382:254-259.

[48] Fornari T, Revision and summary of the group contribution equation of state parameter table: Aplication to edible oil constituents. Fluid Phase Equilib. 2007;262:187-209.